Clays and Clay Minerals, Vol. 53, No. 4, 348–360, 2005.

EXPERIMENTAL EVIDENCE FOR Ca-CHLORIDE ION PAIRS IN THE INTERLAYER OF MONTMORILLONITE. AN XRD PROFILE MODELING APPROACH

ERIC FERRAGE[1,2,*,†], CHRISTOPHE TOURNASSAT[2,3], EMMANUEL RINNERT[2,4], LAURENT CHARLET[1] AND BRUNO LANSON[1]

[1] Environmental Geochemistry Group, LGIT-Maison des GéoSciences, CNRS – Joseph Fourier University, P.O. Box 53, 38041 Grenoble Cedex 9, France

[2] ANDRA, Parc de la Croix Blanche, 1/7 rue Jean Monnet, 92298 Châtenay-Malabry Cedex, France

[3] BRGM, 3 avenue Claude Guillemin, 45060 Orléans Cedex 2, France

[4] Laboratoire de Chimie Physique et Microbiologie pour l'Environnement, UMR 7564 CNRS-Université Henri Poincaré, 405 rue de Vandœuvre, 54600 Villers-Lès-Nancy, France

Abstract—Montmorillonite was equilibrated with high normality Cl^- solutions to assess the possible presence of $MeCl^+$ ion pairs in smectite interlayers suggested by chemical modeling of cation exchange experimental studies. Structural modifications induced by the presence of such ion pairs, and more especially those related to smectite hydration properties, were characterized from the modeling of experimental X-ray diffraction (XRD) profiles. As compared to those obtained from samples prepared at low ionic strength, XRD patterns from samples equilibrated in high ionic strength $CaCl_2$ solutions exhibited a small positional shift of 00*l* basal reflections indicating a greater layer thickness. The rationality of basal reflection positions is also improved and the width of these reflections is decreased. These qualitative modifications are related to the existence of a more homogeneous hydration state with the sole presence at 40% relative humidity (RH) of bi-hydrated smectite layers (2W layers) in high ionic strength samples. By contrast, layers with contrasting hydration states coexist in samples prepared at low ionic strength. The stability of this homogeneous 2W hydration state is also extended towards low RH values in the sample prepared at high ionic strength.

In addition, the intensity distribution is modified in samples prepared at high ionic strength as compared to those obtained at low ionic strength. In particular the relative intensity of the 002 reflection is strongly enhanced in the former samples. This modification arises from an increased electron density in the interlayer mid-plane of 2W layers which is best explained by the presence of cation-chloride ion pairs replacing the divalent cations occupying this structural position in low ionic strength samples. The increased amounts of interlayer species (ion pairs and H_2O molecules), which are confirmed by near-infrared diffuse reflectance spectroscopy results, and the larger size of $CaCl^+$ pairs as compared to Ca^{2+} cations lead to a more stable layer thickness, probably as a result of decreased layer corrugation. Consistent results were obtained for Sr and Mg cations.

Key Words—Ion Pairs, Montmorillonite, XRD Profile Modeling.

INTRODUCTION

Bentonite, a clay material comprising mainly smectite, is considered a potential engineered barrier material for nuclear waste disposal. In high- and intermediate-level long-lived radioactive wastes (ILLW) disposal sites, one possible disposal method involves vitrified waste placed in containers and overpacks, encased in exogenous materials (near-field engineered barrier) and buried in a clay-rich geological formation (far-field barrier). The potential of smectite as near- to far-field barrier material arises from the combination of mechanical self-healing ability, low hydraulic conductivity and high sorption capacities. The last feature is expected to prevent or to delay radionuclide migration. However, the initial properties of smectite could be significantly altered as a consequence of storage-induced perturbations. For example, the use of concrete for waste overpacks or the oxidation of pyrite, which is often present as an accessory mineral in the geological environment, can induce a wide pH range in solutions in contact with the clay barriers. Such perturbations of the solution chemistry might lead to structural changes affecting both the geological host formation and the engineered clay barrier.

An octahedral sheet sandwiched by two tetrahedral sheets forms a smectite layer. Substitutions in either tetrahedral or octahedral sites induce a permanent negative layer charge, balanced by the presence of hydrated interlayer cations. The relationship between interlayer cation composition and the composition of the solution in contact with clay surfaces has been studied for decades, and cation exchange thermodynamics has been developed to model the composition in the clay interlayers (Vanselow, 1932a, 1932b; Sposito, 1977, 1981, 1984; Elprince *et al*., 1980; Shainberg *et al*., 1980;

* E-mail address of corresponding author:
e.ferrage@nhm.ac.uk
† Present address: Department of Mineralogy, The Natural History Museum, Cromwell Road, London SW7 5BD, UK
DOI: 10.1346/CCMN.2005.0530403

Sposito *et al*., 1981; Fletcher and Sposito, 1989 and references therein). In the 1980s, Sposito *et al*. (1983a, 1983b) first suspected the sorption of cation-chloride ion pairs from the comparison between Mg-Na and Ca-Na exchange experiments performed in perchlorate and chloride anionic backgrounds. High exchange selectivity coefficients were found for these complex monovalent cations as compared to simple monovalent cations (Fletcher and Sposito, 1989). The relevance of this cation-anion-clay interaction model was further questioned by various exchange experiments (Suarez and Zahow, 1989; Rhue and Reve, 1990) producing conflicting data and various conceptual models. Despite a detailed analysis of the source of apparent conflicts between these data (Sposito, 1991), due principally to experimental conditions such as clay content, cation-chloride ion pairs are usually not considered in thermodynamic exchange calculations. Sorption of cation-chloride ion pairs in the interlayer of clay minerals was confirmed recently by cation exchange experiments (Tournassat *et al*., 2004a, 2004b) and from the modeling of the interlayer composition in clay particles equilibrated with seawater (Charlet and Tournassat, 2005). These authors also suspected the presence of $CaOH^+$ ion pairs as exchangeable cations at high pH. Similarly, recent studies by nuclear magnetic resonance have revealed the coexistence of Cd^{2+} and $CdCl^+$ in the interlayers of smectites equilibrated in high-concentration Cd chloride solutions (Di Leo and O'Brien, 1999; Di Leo and Cuadros, 2003). However, the locations of sorbed cation-chloride and cation-hydroxide ion pairs were not readily identified by spectroscopy or diffraction methods as opposed to other cations (Hyun *et al*., 2000; Schlegel *et al*., 2001).

The impact of smectite interlayer composition on smectite hydration has been studied extensively using XRD from the positions of 00*l* basal reflections. With increasing moisture in its environment, smectite expands in different steps, corresponding to the intercalation of 0, 1, 2 or 3 sheets of H_2O molecules in the interlayer (Nagelschmidt, 1936; Bradley *et al*., 1937; Mooney *et al*., 1952; Norrish, 1954; Walker, 1956). From these pioneer studies, it is now commonly accepted that the expandability of 2:1 phyllosilicates is controlled by factors such as the nature of interlayer cations, the layer charge and its location (octahedral *vs*. tetrahedral). These general observations have led to different models in which crystalline swelling is controlled by a balance between the repulsive forces due to 2:1 layers interactions and the attractive forces between hydrated interlayer cations and the negatively charged surface of siloxane layers (Norrish, 1954; van Olphen, 1965; Kittrick, 1969a, 1969b; Laird, 1996, 1999). The development of XRD modeling techniques allows these observations to be refined by investigating defective structures such as those resulting from the coexistence of layers having different thicknesses (Ben Brahim *et al*., 1983, 1984; Bérend *et al*., 1995; Cases *et al*., 1997; Cuadros, 1997). Ferrage *et al*. (2005a, 2006) used a similar modeling approach to determine the hydration properties of montmorillonite and beidellite and observed that (1) the nature of the interlayer cation and its ability to sorb water molecules determines the layer thickness of the bi-hydrated and monohydrated layers and confirmed that (2) relative proportions of the different layer types, which correspond to different hydration states, are determined by smectite layer charge and charge location.

The present work aims to characterize the variation of montmorillonite hydration state as a function of the anionic background in order to improve understanding of smectite reactivity in disturbed chemical conditions, such as those expected to occur in near- and/or far-field barriers. From XRD data, the present study focuses on the effect of chloride on Ca-exchanged montmorillonite to assess the presence of cation-chloride ion pairs in the smectite interlayer. Additional near-infrared diffuse reflectance (NIR-DR) spectroscopy data were used to study the local arrangement of H_2O molecules around interlayer species.

MATERIALS AND METHODS

Sample preparation

The smectite used for this study is the SWy-2 montmorillonite reference from the Source Clays Repository of The Clay Minerals Society with structural formula (Stucki *et al*., 1984): $[(Al_{3.01}Fe_{0.43}Mg_{0.56})(Si_{7.97}Al_{0.03})O_{20}(OH)_4]M^+_{0.72}$. This montmorillonite is originally Na-saturated, and exhibits a low octahedral charge and extremely limited tetrahedral substitutions (Mermut and Lagaly, 2001).

Size fractionation was performed by centrifugation to obtain a suspension of the <2 μm size fraction. Ion-exchange processes were achieved on this clay separate at room temperature with 1 mol L^{-1} aqueous saline solutions of $MeCl_2$ (*Me* = Ca, Sr or Mg) or of NaCl prepared from analytical grade reagents and deionized water (milli-Q/18.2 MΩ cm^{-1}). SWy-2 suspensions in these saline solutions were shaken mechanically for 24 h before separation of the solid fraction by centrifugation and addition of fresh saline solution. These steps were repeated three times to ensure a complete cation exchange. Then high ionic strength background samples (HIS-*Me*-SWy) were prepared by direct filtration of the clay suspension whereas for low ionic strength background samples (LIS-*Me*-SWy), excess salt was washed out by four 24 h cycles that included sedimentation, removal of the supernatant and immersion in deionized water.

Choice of experimental conditions

In $CaCl_2$ ion background and according to the selectivity coefficients obtained by Fletcher and Sposito (1989) and recently refined by Charlet and

Tournassat (2005), Ca^{2+} should be the sole Ca interlayer species when the ionic strength value (I) is <0.01 mol L^{-1}, whereas $CaCl^{+}$ presumably becomes the unique interlayer cation when I is >2 mol L^{-1}. A similar behavior is expected for Sr and Mg salts. In the present study, LIS-*Me*-SWy and HIS-*Me*-SWy samples (*Me* = Ca, Sr or Mg) were thus prepared at I <0.01 mol L^{-1} and I = 2.7 mol L^{-1} (corresponding to a total normality of 1 mol L^{-1} $MeCl_2$ solution), respectively, so that the interlayer composition of smectite differs entirely from one set of samples to the other. LIS-Na-SWy and HIS-Na-SWy samples were prepared following the same procedure.

X-ray diffraction

For XRD analysis, suspension aliquots were poured through a Millipore filter (0.4 μm) and the resulting clay films were transferred onto a weighed glass slide. The oriented preparations obtained were then dried at room temperature and the mass of montmorillonite on the glass slide was measured for XRD modeling purposes. The XRD patterns were then recorded using a Bruker D5000 diffractometer equipped with an Ansyco rh-plus 2250 humidity control device coupled to an Anton Paar TTK450 chamber. Experimental measurement parameters were a 0.04º2θ step size and 6 s counting time per step. The divergence slit, the two Soller slits, antiscatter and resolution slits were 0.5º, 2.3º, 2.3º, 0.5º and 0.06º, respectively.

For each sample, XRD patterns were recorded over a time span that did not exceed 2 days after glass slide preparation to avoid kinetically driven dehydration of the montmorillonite. A 15 min waiting period was observed before XRD data collection to ensure hydration equilibration at the desired relative humidity (RH).

X-ray diffraction modeling

Experimental XRD patterns were fitted using a trial-and-error approach and the program initially developed by Drits and Sakharov (1976). Instrumental and experimental factors such as horizontal and vertical beam divergences, goniometer radius, slide length and sample thickness were measured and introduced without further refinement. The linear absorption coefficient (μ*) and z-coordinates within the 2:1 silicate layer were set as recommended by Moore and Reynolds (1997). The distribution of coherent scattering domain sizes (N) was assumed to be lognormal and characterized by its mean value (Drits *et al.*, 1997b). The Sigmastar parameter (σ*), which corresponds to the distribution of particle orientation in the sample, was considered as a variable parameter (Moore and Reynolds, 1997). A σ_z parameter, which corresponds to atomic position fluctuations leading to a disorder of the second type (Guinier, 1964; Drits and Tchoubar, 1990), was also refined. This parameter can be described as the standard deviation of the layer thickness from a mean value.

The three layer types corresponding to the hydration states reported for montmorillonite in non-saturated conditions are the following: dehydrated (0W) layers with interlayer cations in the interlayer mid-plane, mono-hydrated (1W) layers with interlayer cations and H_2O molecules in the same central plane, and bi-hydrated (2W) layers with the central cation plane sandwiched between two planes of H_2O molecules at a distance of 1.2 Å along the c* axis (Ferrage *et al.*, 2005a). The quality of fit to the experimental patterns was assessed using the Rp parameter (Howard and Preston, 1989). This unweighted parameter was chosen as being mostly influenced by intense peaks such as the 001 reflection, where most information on the relative proportions of different layer types and on their thickness is concentrated. Calculated XRD patterns are cut at ~5º2θ (CuKα) because of significant background discrepancies over the low-angle region, possibly resulting from an incorrect description of crystalline defects as proposed by Plançon (2002). However, the profiles of the 00l reflections calculated using either model are similar and the low-angle misfit does not challenge the results obtained in the present study (Ferrage *et al.*, 2005a).

Near-infrared diffuse reflectance analysis

Near-infrared diffuse reflectance spectra were recorded using a Perkin Elmer 2000 FTIR spectrometer equipped with a deuterated triglycine sulfate (DTGS) detector, a tungsten-halogen source and a quartz beam splitter. Spectra were collected using a spectral resolution of 8 cm^{-1}. The optical device used is based on the Harrick© equipment. Diffuse reflectance spectra were recorded from 4000 to 8000 cm^{-1} as the sum of 50 individual scans. Samples were placed in a Harrick© cell in which temperature and pressure were controlled from 25 to 100ºC and from 10^{-4} to 10^{5} Pa, respectively. Sample temperature was measured by a Pt resistance which allows measurements with an accuracy better than 0.1ºC. Spectra of hydrated samples were first recorded before pumping, when samples were equilibrated with room humidity, which was equal to (40±5)%. Samples were subsequently out-gassed at 60ºC for 16 h under a residual pressure of $\sim 5 \times 10^{-3}$ Pa and spectra were then recorded at 25ºC under a residual pressure of 5×10^{-4} Pa. The reported diffuse reflectance, R, is defined as:

$$R = -\log \frac{I_S^D(\sigma)}{I_0^D(\sigma)} \quad (1)$$

where I_S^D is the measured diffused irradiance of the sample, I_0^D the measured diffused irradiance of the reference, and σ the wavenumber. The reference was taken at 24.8ºC from a KBr powder dried under a residual pressure of 5×10^{-3} Pa.

For clay samples, the spectral domain presented in this study can be split in two regions. From 4550 to

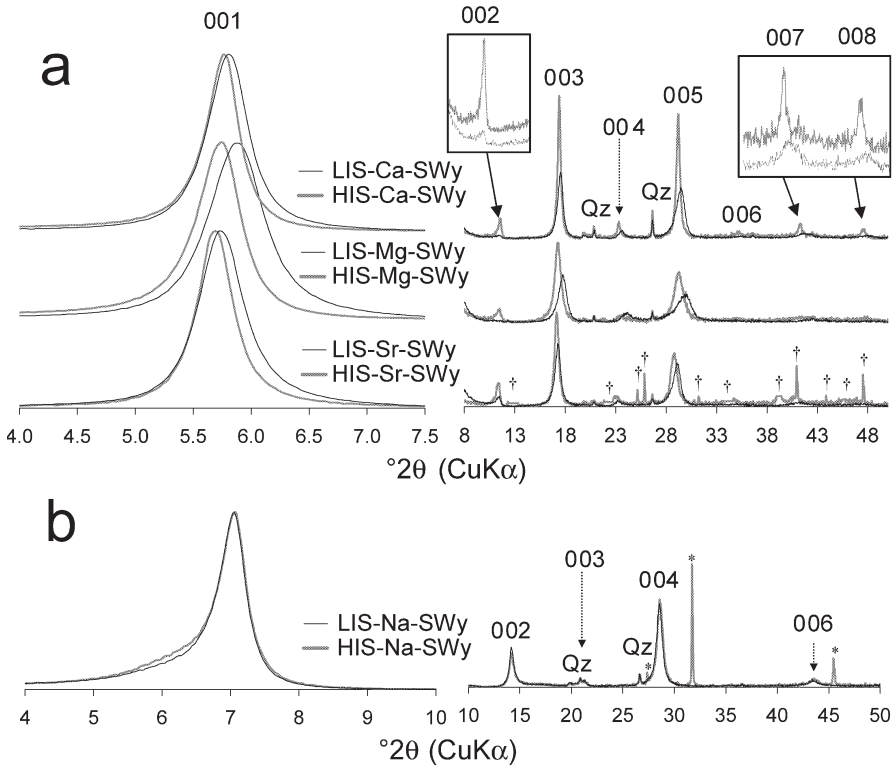

Figure 1. Experimental XRD patterns obtained for the LIS- and HIS-*Me*-SWy samples. (a) *Me* = Ca, Mg, and Sr. (b) *Me* = Na. Intensities in the high-angle region (8−50º2θ) are scaled up (× 15 in a and × 5 in b). The 002, 007 and 008 reflections are scaled up for the LIS- and HIS-Ca-SWy samples. Quartz, $SrCl_2$ and NaCl impurities are marked as Qz, † and *, respectively.

5500 cm^{-1}, only H_2O molecules can be observed from the combinations of stretching and bending modes. From 6500 to 7500 cm^{-1}, overtones of stretching modes of all OH groups, both from interlayer H_2O molecules and from the silicate framework, are visible (Burneau *et al*., 1990; Madejová *et al*., 2000b). In previous IR studies of smectites, fundamental stretching modes have been reported over the 3370−3670 cm^{-1} range (Madejová *et al*., 2000; Vantelon *et al*., 2001; Bishop *et al*., 2002). Consequently, the frequency range calculated for the first stretching overtone extends from 6575−7175 cm^{-1}, with an 82.5 cm^{-1} anharmonicity coefficient for OH groups (Burneau and Carteret, 2000).

RESULTS AND DISCUSSION

Qualitative description of LIS- and HIS-Me-SWy XRD patterns

The XRD patterns recorded at 40% RH for LIS- and HIS-Ca-SWy samples are shown in Figure 1a, and d_{001} values and departure from rationality, ξ, calculated as the standard deviation of $l \times (00l)$ values, are reported in Table 1. An increased ξ parameter is indicative of interstratified structures.

A small shift of the 001 reflection towards lower angles is visible for the XRD pattern of sample HIS-Ca-SWy as compared to sample LIS-Ca-SWy, corresponding to a small increase of layer thickness rather than to a lower coherent scattering domain size (CSDS) along the *c** axis as peak width is lower for sample HIS-Ca-SWy than for sample LIS-Ca-SWy. An intensity increase of 002, 003, 004 and 005 reflections, together with their sharpening, is also visible on the XRD pattern of sample HIS-Ca-SWy as compared to sample LIS-Ca-SWy. Finally, the lower ξ parameter measured for sample HIS-Ca-SWy indicates a more homogeneous hydration

Table 1. Basal reflection qualitative describers (position and rationality) determined for LIS- and HIS-*Me*-SWy samples (*Me* = Ca, Mg, Sr and Na) at 40% RH. The 001 reflection position (d_{001}) is given in Å. The ξ parameter (Å) which accounts for the departure from rationality of the 00*l* reflection series is calculated as the standard deviation of the $l \times d(00l)$ values calculated for the X_i measurable reflections over the 2−50º2θ CuKα angular range.

Sample	d_{001}	ξ/X_i
LIS-Ca-SWy	15.23	0.15/5
HIS-Ca-SWy	15.32	0.03/8
LIS-Mg-SWy	15.03	0.09/5
HIS-Mg-SWy	15.40	0.12/8
LIS-Sr-SWy	15.40	0.09/5
HIS-Sr-SWy	15.53	0.04/5
LIS-Na-SWy	12.54	0.04/4
HIS-Na-SWy	12.54	0.04/4

state in this sample as compared to sample LIS-Ca-SWy. To verify that the observed modifications are not related to the ionic strength of the suspension, the same experiment was performed on samples LIS-Na-SWy and HIS-Na-SWy and identical XRD patterns, within experimental reproducibility, were obtained for the two samples (Figure 1b, Table 1).

For samples LIS- and HIS-Mg-SWy as well as for samples LIS- and HIS-Sr-SWy, observations similar to those reported for samples LIS- and HIS-Ca-SWy were made (Figure 1a). However for sample HIS-Sr-SWy, the presence of $SrCl_2$ salt precipitation prevents the precise observation of the high-angle XRD pattern region. A d_{001} increase is observed from 15.03 Å for sample LIS-Mg-SWy to 15.40 Å for sample HIS-Mg-SWy, and from 15.40 Å for sample LIS-Sr-SWy to 15.53 Å for sample HIS-Sr-SWy, this increase being systematically associated with a sharpening of the 001 reflection (Table 1, Figure 1a). In addition, the ξ parameter decreases for sample HIS-Sr-SWy compared to sample LIS-Sr-SWy, whereas it increases slightly for HIS-Mg-SWy as compared to LIS-Mg-SWy (Table 1). However, the ξ parameters determined for all samples are low (<0.15 Å) implying nearly homogeneous hydration states in all cases. Similar peak positions and ξ parameters were obtained for LIS- and HIS-Na-SWy samples (Table 1).

Origin of the observed structural changes

Hydration homogeneity and layer fluctuation. To assess further the hydration homogeneity, the full width at half maximum intensity (FWHM) of all measurable 00*l* reflections is plotted as a function of the *l* index, after correction by a cosθ factor to compensate for particle-size broadening (Figure 2). For a given sample (LIS- or HIS-*Me*-SWy) all FWHM values are aligned. If different layer types were interstratified in the samples, such a steady broadening of 00*l* reflections would not be observed. Rather, interstratification of layers exhibiting different layer thickness values as a result of their contrasting hydration states would lead to a random broadening of 00*l* reflections as a function of the *l* index. For a given 00*l* reflection, this broadening can be predicted from Méring's principle (Méring, 1949; Moore and Reynolds, 1997).

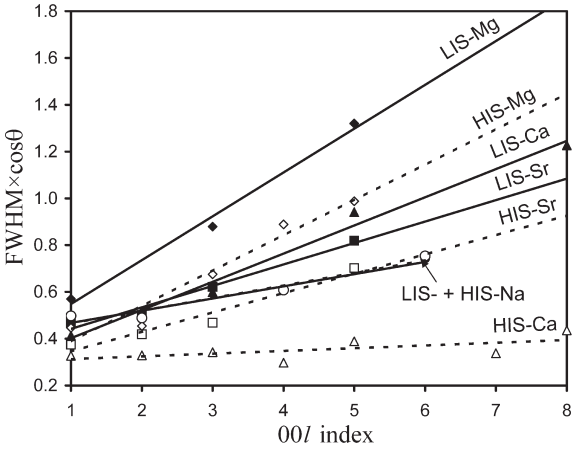

Figure 2. Evolution of the full width at half maximum intensity (FWHM) measured on the 00*l* basal reflection as a function of the *l* index the for LIS- and HIS-*Me*-SWy samples (solid and dashed lines, respectively, *Me* = Ca, Mg, Sr and Na).

The high hydration homogeneity of the different samples deduced from both the low ξ values and from the linear dependence of the 00*l* reflection FWHMs on the *l* index makes it possible to interpret the slopes of the linear correlations shown in Figure 2 as indicative of layer-thickness fluctuations. These fluctuations are similar to strains and induce peak broadening of 00*l* reflections steadily increasing with *l* index (Kodama *et al.*, 1971). The slope of this linear correlation is dramatically decreased for sample HIS-Ca-SWy as compared to sample LIS-Ca-SWy, thus indicating a smaller layer thickness variability for the former sample. For LIS- and HIS-Mg-SWy samples on the one hand and for LIS- and HIS-Sr-SWy samples on the other, the slopes of the linear correlations are similar even though samples prepared with Sr and Mg in a high ionic strength background (HIS-Sr-SWy and HIS-Mg-SWy) have smaller FWHM values than the corresponding samples prepared in a low ionic strength background (LIS-Sr-SWy and LIS-Mg-SWy). Similar evolutions of basal reflection FWHM were observed as a function of the *l* index for LIS- and HIS-Na-SWy samples (Figure 2).

Distribution of intensity. Another significant feature of experimental patterns recorded for LIS- and HIS-*Me*-SWy samples is the intensity modification of 00*l* reflections and especially that of the 002 reflection, which is strongly increased in HIS-*Me*-SWy samples compared to the corresponding LIS-*Me*-SWy samples. As discussed above, similar high hydration homogeneity is expected for all samples, and reflection intensity is directly related to the structure factor of the main layer type, which in turn includes the scattering factors of all its constituent atoms. As a consequence, the structure factor of the different 00*l* reflections and thus their intensity ratio are modified if additional elements are introduced in montmorillonite interlayers. If smectite interlayers incorporated $MeCl^+$, the increase in electronic density compared to interlayer Me^{2+} species would result both from the presence of Cl^- anions and from the monovalent character of the $MeCl^+$ ion pair. As a result, the amount of interlayer species would have to be doubled to compensate for the permanent layer charge deficit. The modification of the electronic density resulting from the presence of monovalent ion pairs compared to divalent cations can be estimated from the number of electrons corresponding to each charge-compensating species. Ca^{2+} cations hold $18e^-$, *i.e.* $9e^-$ per charge unit (c.u.). This index (η) corresponds to the atomic scattering factor for θ = 0 weighted for the cation

valency. As Cl^- anions hold $18e^-$, $CaCl^+$ ion pairs have $36e^-$/c.u. Similar calculations for other divalent cations lead to the following values: $\eta Mg^{2+} = 6e^-$/c.u., $\eta MgCl^+ = 30e^-$/c.u., $\eta Sr^{2+} = 18e^-$/c.u. and $\eta SrCl^+ = 54e^-$/c.u. In agreement with this basic approach, the integrated intensity ratio between 002_{MeCl^+} and $002_{Me^{2+}}$ reflections is linearly correlated to the η ratio between the two compensating species ($\eta MeCl^+/\eta Me^{2+}$, Figure 3). This correlation suggests the presence of cation-chloride ion pairs in the interlayers of HIS-*Me*-SWy samples.

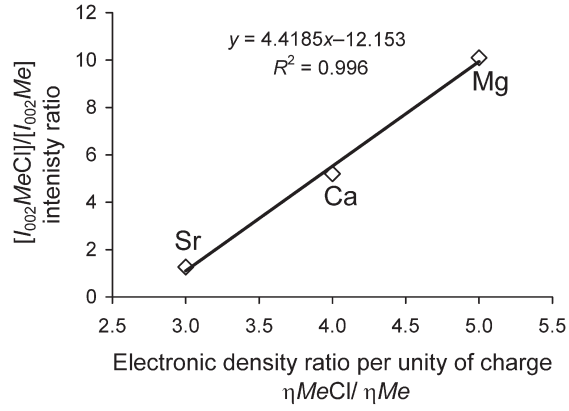

Figure 3. Intensity ratio of 002 reflections measured on the LIS- and HIS-*Me*-SWy XRD patterns as a function of the scattering factor ratio (η) between $MeCl^+$ and Me^{2+} interlayer species (*Me* = Ca, Mg or Sr), weighted for their valency (see text for details).

LIS- and HIS-Ca-SWy XRD profile modeling

The possible presence of $CaCl^+$ ion pairs in smectite interlayers may be further assessed from modeling the whole experimental XRD patterns. For each pattern modeling, two mixed-layer structures (MLSs) that can contain one (periodic structure), two or three layer types (0W, 1W, 2W) randomly interstratified (R = 0) were considered to account for the hydration heterogeneity. The presence of two MLSs does not imply that two populations of particles are physically present in the sample. Due to layer-charge distribution, the smectite structure may incorporate layers exhibiting different hydration states as a function of the relative humidity (Ferrage *et al*., 2005a, 2006). As a result, special care was given to ensure strictly identical chemical composition and atomic *z*-coordinates for each layer type, as well as sigmastar σ*, and σ_z in the two MLSs.

The strategy used for XRD profile modeling has been to mimic as closely as possible the 001 reflection with a MLS as homogeneous as possible, *i.e*. containing as few different layer types as possible. If it proved necessary in order to obtain a good fit, a second MLS was introduced to fill the gaps between calculated and experimental patterns, and to account for the hydration heterogeneity of the sample better. Finally, the structure of the different layer types, and more especially their interlayer structure, was refined to reproduce the intensity distribution over the whole angular range.

Sample LIS-Ca-SWy. Qualitatively, the XRD pattern of sample LIS-Ca-SWy recorded at 40% RH exhibits diffraction maxima forming an almost rational series corresponding to 2W layers. Asymmetries on the high-angle side of the 001 reflection and on the low-angle side of the 005 reflection indicate the interstratification of other layer types (Figure 1). Accordingly, two structures were used to fit the experimental XRD pattern (Figure 4). The first one contains only 2W layers (layer thickness = 15.18 Å; Figure 4a, Table 2). This first periodic structure allows most features of the experimental XRD pattern to be reproduced, but the residual trace shows that the asymmetries described above were not reproduced (Figure 4a). A second contribution (60:30:10 ratio for 2W, 1W and 0W layers, respectively) was thus added. The XRD profile calculated for this additional MLS exhibits a 001 reflection shifted toward the high-angle side compared to the pure 2W phase because of the presence of layers with smaller layer thickness (0W and 1W layers, Figure 4b). Mixing 87% of the first structure with 13% of the second allows the experimental pattern to be fitted satisfactorily (Rp = 1.45%, Figure 4c). The optimum fit to the experimental XRD patterns was obtained assuming for 2W layers the configuration of smectite interlayer species proposed by Ferrage *et al.* (2005a). This structure model includes a unique plane of H_2O molecules located at 1.20 Å, along

Table 2. Optimum structural parameters used for the simulation of XRD profiles obtained for LIS- and HIS-Ca-SWy samples. Both calculated patterns include the contributions of two structures (S), relative abundance (Ab) and layer thickness (LT) of each layer type (2W, 1W and 0W), given in % and in Å, respectively. Amounts of interlayer H_2O molecules and cations are given per unit-cell. *N*, σ* and σ_z indicate the size of the CSDs along the *c** axis, the deviation of particle orientation, and the fluctuation of layer thickness, respectively.

Sample	Ab	Ab 2W	Ab 1W	Ab 0W	LT 2W	LT 1W	LT 0W	*N* (layers)	σ* (°)	σ_z (Å)	Cations	nH_2O 2W	nH_2O 1W
LIS-Ca-SWy	87	100	0	0	15.18	–	–	8.7	6.5	0.35	0.36 Ca^{2+}	2 × 3.2	–
	13	60	30	10	15.18	12.60	10.00	8.7	6.5	0.35	0.36 Ca^{2+}	2 × 3.2	3.6
HIS-Ca-SWy	80	100	0	0	15.295	–	–	10.5	6.2	0.00	0.72 $CaCl^+$	2 × 3.7	–
	20	100	0	0	15.295	–	–	5.0	6.2	0.00	0.72 $CaCl^+$	2 × 3.7	–

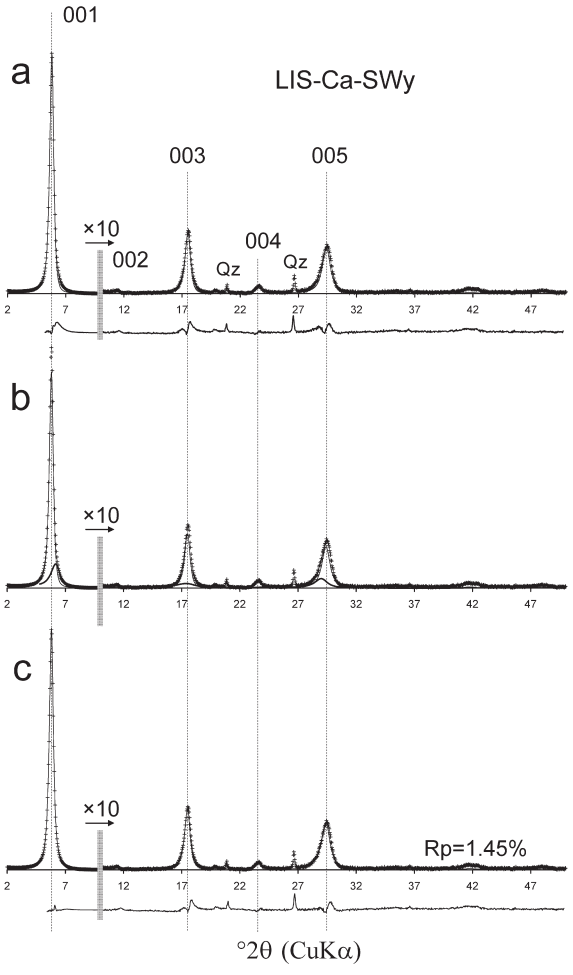

Figure 4. Modeling of XRD patterns recorded at 40% RH for sample LIS-Ca-SWy. The gray bar indicates the scaling up ($\times 10$) of the high-angle region intensities. The experimental pattern is shown as crosses whereas the calculated patterns and difference plots are shown as solid lines. (a) XRD pattern calculated for a pure bi-hydrated periodic structure. (b) XRD pattern calculated for a MLS structure containing 60%, 30% and 10% of 2W, 1W and 0W, respectively. (c) Optimum fit to the experimental pattern, corresponding to the combination of the above two structures in an 87:13 ratio.

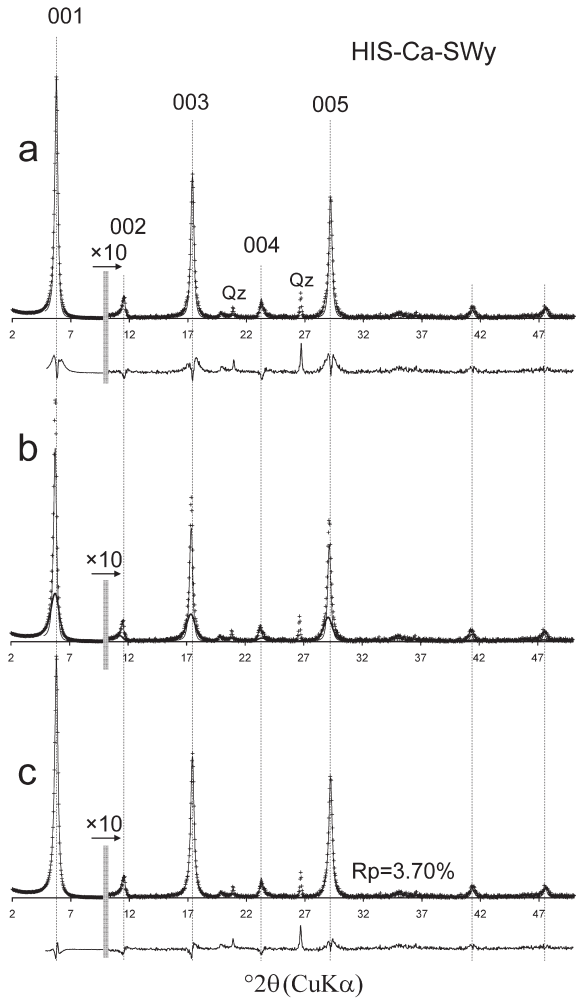

Figure 5. Modeling of XRD patterns recorded at 40% RH for sample HIS-Ca-SWy. The gray bar indicates the scaling up ($\times 10$) of the high-angle region intensities. The experimental pattern is shown as crosses whereas the calculated patterns and difference plots are shown as solid lines. (a) XRD pattern calculated for a pure bi-hydrated structure with an average CSDS along the c^* axis of 10.5 layers. (b) XRD pattern calculated for a pure bi-hydrated periodic structure with an average CSDS along the c^* axis of 5.0 layers. (c) Optimum fit to the experimental pattern, corresponding to the combination of the above two structures in an 80:20 ratio.

the c^* axis on either side of the interlayer mid-plane which contains exclusively interlayer Ca^{2+} cations.

Sample HIS-Ca-SWy. As compared to sample LIS-Ca-SWy, an increase of layer thickness for 2W layers and a decrease of layer thickness fluctuation (σ_z) can be deduced from the qualitative description of the experimental XRD pattern recorded at 40% RH. Moreover, the extremely small value determined for the ξ parameter indicates an increased homogeneity of the hydration state. However, two structures were necessary to fit the experimental XRD pattern. These two structures differ from those obtained for sample LIS-Ca-SWy (Figure 5), as they both contain only 2W layers, differing only by their respective CSDSs (10.5 and 5.0 layers, respectively). This structural similarity arises from the discrepancies observed between the experimental pattern and that calculated for the first 2W periodic structure which are symmetrical on each side of the calculated diffraction maxima (Figure 5a). Mixing the two contributions (80:20 ratio for the first and second periodic structures, respectively), leads to a satisfactory fit to the experimental pattern (Rp = 3.70%; Figure 5c, Table 2). In both structures, the layer thickness of 2W layers is increased from 15.18 (sample LIS-Ca-SWy) to 15.295 Å (sample HIS-Ca-SWy). The amount of interlayer H_2O

molecules is also increased from 2×3.2 (sample LIS-Ca-SWy) to 2×3.7 (Table 2, Figure 5a). In addition, the σ_z parameter, corresponding to layer-thickness fluctuation, is found now to be equal to zero, in agreement with the constant FWHM values determined for 00*l* reflections (Figure 2). To account for the increased intensity of the 002 reflection recorded for sample HIS-Ca-SWy (as compared to sample LIS-Ca-SWy sample), the interlayer structure of 2W layers had to be modified from the model used to fit sample LIS-Ca-SWy. This model includes a central cation plane sandwiched between two planes of H_2O molecules at a distance of 1.2 Å along the *c** axis (Ferrage *et al.*, 2005a). For sample HIS-Ca-SWy, the electron density had to be increased specifically in the interlayer mid-plane, where interlayer cations are located. Two models can give rise to such an increased electron density.

In the first model, the scattering power of interlayer cations located in the interlayer mid-plane is increased, either by increasing their amount, with the strong constraint of the layer charge balance, or by increasing their specific scattering power. Both effects had to be combined to reproduce satisfactorily the experimental data. Accordingly, the optimum fit to the experimental XRD pattern of sample HIS-Ca-SWy was obtained assuming for 2W layers the configuration of smectite interlayer species proposed by Ferrage *et al.* (2005a), and the sole presence of $CaCl^+$ ion pairs in the interlayer mid-plane. Consistently, the number of monovalent $CaCl^+$ ion pairs was twice that of Ca^{2+} in sample LIS-Ca-SWy.

In the second model, additional neutral interlayer species, such as H_2O molecules for example, have to be introduced in the interlayer mid-plane in addition to interlayer Ca^{2+} cations, thus leading to a dramatically different interlayer structure. To fit the experimental data, the electron density in the interlayer mid-plane should be equivalent to that in the first model (presence of 0.72 $CaCl^+$ ion pairs per unit-cell) and ~2.3 H_2O molecules should thus be present in this interlayer mid-plane in addition to Ca^{2+} cations (0.36 per unit-cell). This second model is not consistent with the interlayer configuration refined by Ferrage *et al.* (2005b) for 2W smectite layers or with any alternative model from the literature and can thus be rejected. Modeling of XRD patterns recorded for LIS-Ca-SWy and HIS-Ca-SWy samples thus provides unambiguous experimental support for the presence of $CaCl^+$ ion pairs in Ca-saturated smectite samples prepared at high ionic strength.

Smectite hydration in LIS- and HIS-Ca-SWy samples

In addition to the sole presence of $CaCl^+$ ion pairs as interlayer cations in samples prepared in high ionic strength $CaCl_2$ background, XRD profile modeling highlighted significant differences in the hydration state of LIS- and HIS-Ca-SWy samples. Specifically, at 40% RH, the latter sample contains only 2W layers (Figure 5, Table 2), whereas different layer types are interstratified in the former sample. This increased homogeneity of hydration properties with increasing density of interlayer cations is reminiscent of the results obtained by Ferrage *et al.* (2006) on two Ca-montmorillonites having contrasting layer-charge deficits, and thus contrasting amounts of interlayer cations. To assess the stability of montmorillonite hydration properties as a function of RH, XRD patterns were recorded at 20% RH for both LIS- and HIS-Ca-SWy samples (Figure 6). For the LIS-Ca-SWy sample, the RH decrease results in a significant decrease of the d_{001} value corresponding to the transition from 2W to 1W layers (Figure 6), in a dramatic broadening of the 001 reflection and in a significant increase of the ξ parameter (1.30 Å). The experimental pattern obtained at 20% RH for sample LIS-Ca-SWy is similar to that obtained by Ferrage *et al.* (2005a), on the <1 μm size fraction of SWy-1 montmorillonite, thus implying similar proportions of the different layer types (ξ = 1.24 Å and 45:40:15 ratio for 2W, 1W and 0W layers, respectively). On the other hand, only a limited shift of d_{001} is visible on the experimental XRD pattern obtained for sample HIS-Ca-SWy at 20% RH as compared to that recorded at 40% RH. This shift is probably related to the decrease of layer thickness for 2W layers with decreasing RH rather than to a significant heterogeneity of hydration properties, as no significant asymmetry is visible for 00*l* reflections. This hypothesis is also supported by the similar low value (0.03 Å) determined for the ξ parameter at this lower RH value. The increased stability range of the bi-hydrated state towards the lower RH value observed for sample HIS-Ca-SWy is consistent with the increased stability of this hydration state with increasing amount of interlayer cations reported by Ferrage *et al.* (2006) for Ca-saturated montmorillonites.

This increased stability of the bi-hydrated state is accompanied at 40% RH by an increased amount of interlayer H_2O molecules from 2×3.2 to 2×3.7 per unit-cell for Ca- and HIS-Ca-SWy samples, respectively (Table 2). NIR-DR spectra were recorded at 40% RH for these two samples to estimate the amount of interlayer H_2O molecules (Figure 7). The combinations of stretching and bending modes are observed at 5250 and 5215 cm^{-1} for LIS- and HIS-Ca-SWy samples, respectively. Overtones of OH-stretching modes from H_2O molecules and structural OH groups are observed at 6830, 7095 cm^{-1} and at 6805, 7065 cm^{-1} for LIS- and HIS-Ca-SWy samples, respectively. Over the two frequency ranges, the increased reflectance measured for sample HIS-Ca-SWy compared to sample LIS-Ca-SWy supports the greater amount of interlayer H_2O molecules in the former sample although no quantitative estimate was performed. From NIR-DR results, the amount of H_2O molecules in sample HIS-Ca-SWy is sufficient to induce a network of H_2O molecules similar to that in liquid H_2O. In addition, profiles of NIR-DR

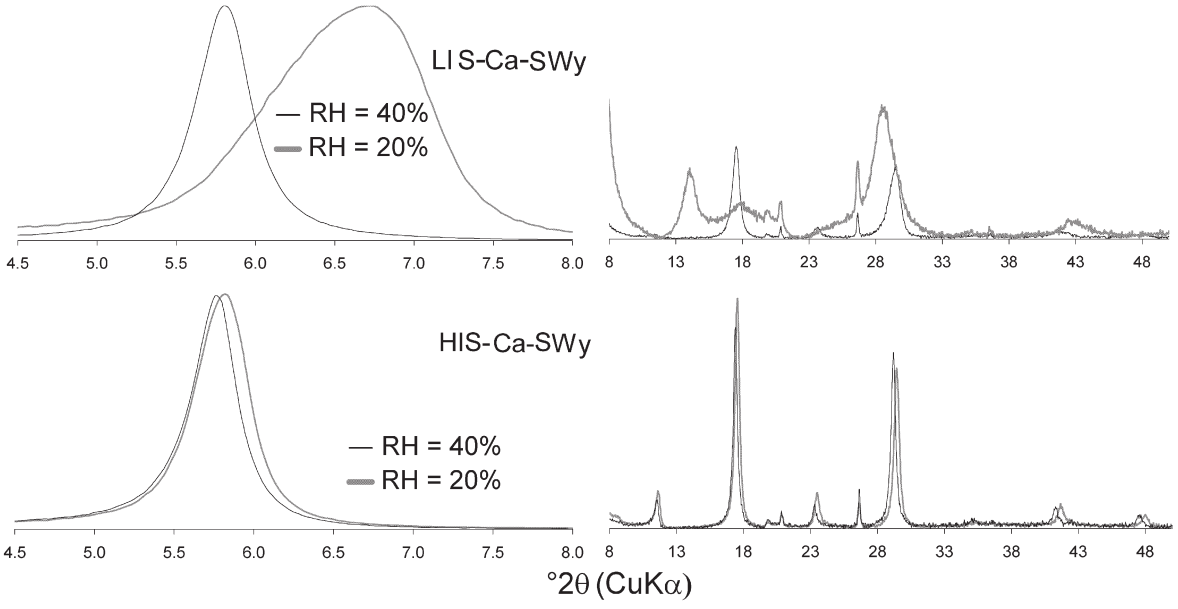

Figure 6. Comparison of experimental XRD patterns recorded for LIS- and HIS-Ca-SWy samples at 40 and 20% RH. Intensities in the high-angle region (8−50°2θ) are scaled up (× 15) in comparison to the low-angle region.

spectra obtained for LIS- and HIS-Ca-SWy samples are significantly different, the latter sample exhibiting a broad combination band compared to sample LIS-Ca-SWy (Figure 7). This broadening is possibly related to the presence of Cl^- anions that affects the local environment of adsorbed H_2O molecules.

Configuration of interlayer H_2O molecules in LIS- and HIS-Me-SWy samples

In addition, the NIR-DR spectroscopy was performed on out-gassed preparations of LIS- and HIS-Ca-SWy samples (Figure 8) to study the configuration of the first hydration sphere around interlayer cations in these samples and to assess the possible influence of Cl^- anions on the interaction between interlayer cation and H_2O molecules. Even under deep-vacuum conditions, some H_2O molecules bound to interlayer cations are still present, as shown by the combination of bending and stretching modes observed at 5240 and 5225 cm^{-1} for out-gassed LIS- and HIS-Ca-SWy samples, respectively (Figure 8). These values may be assigned to strongly disturbed H_2O molecules from the first hydration shell of interlayer cations. Bands observed at 6910, 7095 cm^{-1} and at 6910, 7100 cm^{-1} for out-gassed LIS- and HIS-Ca-SWy samples, respectively, are assigned to the overtones of H_2O molecules and layer OH-stretching mode. From the comparison of the reflectance intensity measured on the combination

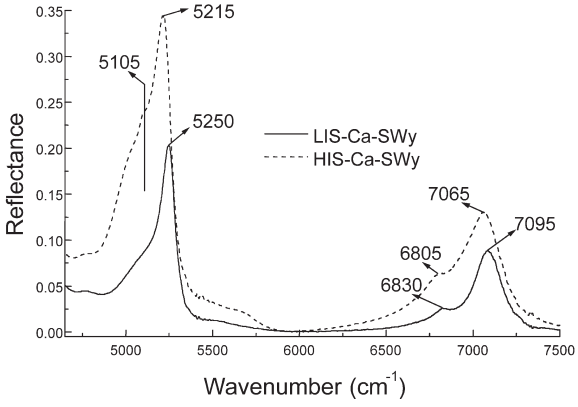

Figure 7. NIR-DRS spectra of LIS- and HIS-Ca-SWy at 40% RH. Solid and dashed lines represent LIS- and HIS-Ca-SWy samples, respectively.

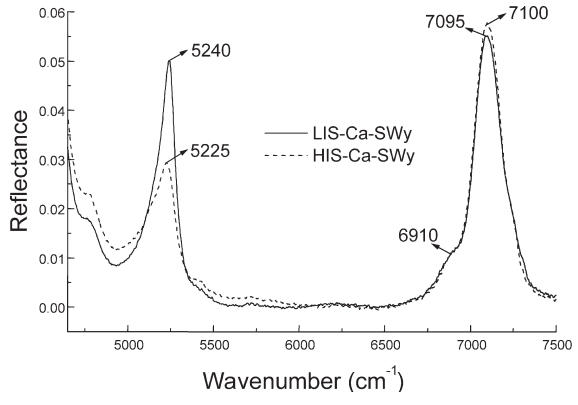

Figure 8. NIR-DRS spectra of out-gassed LIS- and HIS-Ca-SWy. Solid and dashed lines represent LIS- and HIS-Ca-SWy samples, respectively.

bands, the amount of H_2O molecules is clearly greater in sample LIS-Ca-SWy than in sample HIS-Ca-SWy, although the amount of cations in the latter sample is presumably twice that in the former sample. This difference may be related to the local perturbation of the H_2O-cation configuration because of the presence of Cl^- anions modifying the affinity of Ca^{2+} cations for H_2O molecules. However, the profiles of the combination bands are rather similar for both samples.

From the qualitative observation of XRD patterns recorded for LIS- and HIS-*Me*-SWy, a peculiar behavior was noted for sample HIS-Mg-SWy (Table 1), this sample being the only one to show an increase of the ξ parameter from sample LIS-Mg-SWy to sample HIS-Mg-SWy (Table 1). This slight increase, which indicates a more heterogeneous structure for the sample prepared at high ionic strength $MgCl_2$ background, can be related to the difficulty of Mg^{2+} cations to exchange part of their H_2O molecules for Cl^-. The distribution of the H_2O molecules in the first hydration shell of cations obtained from molecular dynamic simulations and wide-angle neutron scattering data (Mazzarella *et al.*, 1967; Dickens and Brown, 1972; Hewish *et al.*, 1982; Spohr *et al.*, 1988) may provide some insight into the contrasting behavior of Mg^{2+} as compared to Ca^{2+} or Sr^{2+}. According to these results, Mg^{2+} cations have a propensity to stick rigidly to a well defined symmetrical octahedron, with short Mg−O(OH) distances, because of their high hydration energy. As a consequence, inner-sphere $MgCl^+$ ion pairs are unlikely to form, although the increased intensity of the 002 reflection is consistent with the exclusive $MgCl^+$ ion pairs as interlayer cationic species (Figure 3). In contrast to Mg^{2+}, Ca^{2+} cations exhibit no regular symmetry in their hydration shells, due to the weak hydration energy of Ca^{2+}. Cl^- anions therefore have an increasing tendency to replace H_2O molecules from the first hydration shell in the sequence Mg^{2+} to Ca^{2+} and Sr^{2+}. Accordingly, the $MgCl^+$ ion pairs may not replace all Mg^{2+} cations in the interlayer of sample HIS-Mg-SWy resulting in the coexistence of two types of 2W layers, one saturated by Mg^{2+} and the other by $MgCl^+$ ions, thus increasing slightly the ξ parameter.

Smectite interlayer structure in LIS- and HIS-Me-SWy samples

From XRD profile modeling results, the hypothetical presence of $CaCl^+$ ion pairs, as compared to Ca^{2+} cations, in montmorillonite interlayers leads to significant differences for the CSDS, for layer thickness of 2W layers, and for the deviation from this modified layer thickness (σ_z, Table 2) in addition to the modified hydration properties described above. Ferrage *et al.* (2005a) showed that the layer thickness depends on the cation ionic radius and on its affinity for H_2O. In the present study, layer thickness determined at 40% RH for 2W layers in sample LIS-Ca-SWy (15.18 Å) is close to that determined earlier (15.11 Å, Ferrage *et al.*, 2005a) whereas that determined for sample HIS-Ca-SWy is considerably increased (15.295 Å). As Ferrage *et al.* (2006) have shown that the interlayer cation density does not appear to influence layer thickness at a given RH value on two natural montmorillonites with contrasting layer charges, the increased layer thickness is probably related to the presence of Cl^- (as $CaCl^+$ ion pairs) rather than to the increased amount of Ca in the interlayer.

However, the increased amount of interlayer cations in sample HIS-Ca-SWy as compared to sample LIS-Ca-SWy leads to an increase of the H_2O content (from 2×3.2 to 2×3.7 per unit-cell, respectively, Table 2). The limited character of this associated increase is probably related to the almost complete filling of the interlayer space in sample HIS-Ca-SWy. This hypothesis is supported by the combined increase of the CSDS and decrease of the σ_z value (Table 2) which consistently indicate considerably smaller layer-thickness variability for 2W layers in sample HIS-Ca-SWy. A possible cause of this decreased disorder in the montmorillonite structure is shown schematically in Figure 9. The incomplete interlayer filling of sample LIS-Ca-SWy may lead to a significant corrugation of the layers resulting from the local balance between attractive (between layer and interlayer cations) and repulsive (between adjacent layers) forces. In the proposed XRD modeling approach, this layer corrugation is accounted for by the σ_z parameter. For sample HIS-Ca-SWy, the more complete filling of the interlayer space leads both to increased layer thickness and to a more homogeneous distribution of interlayer species. As a result, local contrasts between interlayer domains containing or not interlayer cations are probably reduced, thus lowering the corrugation of the layers (Figure 9) and the fluctuation of layer thickness as observed experimentally.

Finally, the impact of the increased amount of interlayer species, and thus of the increased interlayer electron density, in HIS-*Me*-SWy samples on the profiles

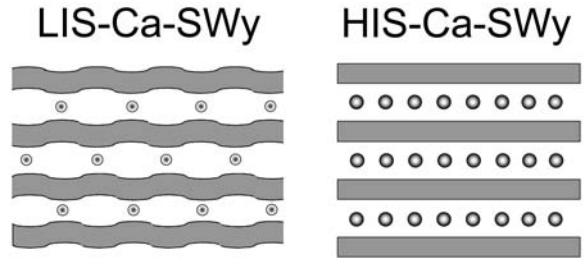

Figure 9. Schematic representation of the influence of $MeCl^+$ ion pairs on smectite interlayers. The incomplete interlayer filling of sample LIS-Ca-SWy (left) leads to a significant corrugation of the layers resulting from the local balance between attractive (between layer and interlayer cations) and repulsive (between adjacent layers) forces. For sample HIS-Ca-SWy (right), the more complete filling of the interlayer space leads both to the increased layer thickness and to a more homogeneous distribution of interlayer species, thus lowering the corrugation of the layers and the fluctuation of layer thickness.

of experimental XRD patterns may be used to assess the presence of such ion pairs. This ability is illustrated in Figure 3 by the linear correlation obtained between the scattering power of interlayer cationic species and the intensity of the 002 reflection measured experimentally. Consequently, this simple measurement can be used as a good indicator of the relative proportion of ion pairs present in the sample, provided that similar amounts of material are deposited on the oriented preparations for both LIS- and HIS-*Me*-SWy samples.

CONCLUSIONS

The present study provides, for the first time, clear XRD experimental support for the presence of $MeCl^+$ ion pairs in the interlayer of expandable clay minerals equilibrated with high normality $MeCl_2$ solutions. This conclusion confirms the need to include these species in cation exchange thermodynamics calculations. Charlet and Tournassat (2005) have successfully modeled the interlayer composition of clay particles equilibrated with seawater, using for these species the exchange selectivity data reported by Tournassat *et al.* (2004b). However, the strong influence of these species in other salty environments may require further refinement of these preliminary parameters.

The possible introduction of $MeCl^+$ ion pairs in smectite interlayers is also of interest for the structural characterization of clay minerals because of the induced modifications of smectite hydration properties. For example, the multispecimen method developed initially by Drits *et al.* (1997a) and Sakharov *et al.* (1999) to characterize mixed-layer minerals requires the fitting of several experimental XRD patterns recorded for the same sample under different conditions, *i.e.* either with different interlayer cations and/or saturation with different polar molecules (H_2O, ethylene glycol, ···) using a single structure model. As a result of these contrasting conditions, the behavior of expandable (smectite) layers is modified, thus providing additional constraints on the structure model. Because saturation of smectite interlayers with $MeCl^+$ ion pairs induces homogeneous hydration of the expandable layers, the number of parameters to be refined is thus reduced for each XRD pattern and a more reliable description of complex clay minerals can thus be obtained.

ACKNOWLEDGMENTS

The results presented in the present article were collected during a PhD thesis granted by ANDRA (French National Agency for Nuclear Waste Disposal). ANDRA is thanked for permission to publish this manuscript and for financial support. The French Geological Survey (BRGM) is acknowledged for its financial support. EF is grateful to Prof. Boris A. Sakharov for fruitful discussions during XRD profile modeling. The manuscript was improved by constructive reviews by two anonymous reviewers, by Associate Editor David A. Laird, and by comments made by Emmanuel Jacquot on an early version of the manuscript.

REFERENCES

Ben Brahim, J., Armagan, N., Besson, G. and Tchoubar, C. (1983) X-ray diffraction studies on the arrangement of water molecules in a smectite. I. Two-water-layer Na-beidellite. *Journal of Applied Crystallography*, **16**, 264–269.

Ben Brahim, J., Besson, G. and Tchoubar, C. (1984) Etude des profils des bandes de diffraction X d'une beidellite-Na hydratée à deux couches d'eau. Détermination du mode d'empilement des feuillets et des sites occupés par l'eau. *Journal of Applied Crystallography*, **17**, 179–188.

Bérend, I., Cases, J.M., François, M., Uriot, J.P., Michot, L.J., Masion, A. and Thomas, F. (1995) Mechanism of adsorption and desorption of water vapour by homoionic montmorillonites: 2. the Li^+, Na^+, K^+, Rb^+ and Cs^+ exchanged forms. *Clays and Clay Minerals*, **43**, 324–336.

Bishop, J., Murad, E. and Dyar, M.D. (2002) The influence of octahedral and tetrahedral cation substitution on the structure of smectites and serpentines as observed through infrared spectroscopy. *Clay Minerals*, **37**, 361–628.

Bradley, W.F., Grim, R.E. and Clark, G.F. (1937) A study of the behavior of montmorillonite on wetting. *Zeitschrift für Kristallographie*, **97**, 260–270.

Burneau, A. and Carteret, C. (2000) Near infrared and ab initio study of the vibrational modes of isolated silanol on silica. *Physical Chemistry Chemical Physics*, **2**, 3217–3226.

Burneau, A., Barrès, O., Gallas, J.P. and Lavalley, J.C. (1990) Comparative study of the surface hydroxyl groups of fumed and precipitated silicas. 2. Characterization by infrared spectroscopy of the interaction with water. *Langmuir*, **6**, 1364–1372.

Cases, J.M., Bérend, I., François, M., Uriot, J.P., Michot, L.J. and Thomas, F. (1997) Mechanism of adsorption and desorption of water vapour by homoionic montmorillonite: 3. The Mg^{2+}, Ca^{2+}, Sr^{2+} and Ba^{2+} exchanged forms. *Clays and Clay Minerals*, **45**, 8–22.

Charlet, L. and Tournassat, C. (2005) Fe(II)-Na(I)-Ca(II) cation exchange on montmorillonite in chloride medium; evidence for preferential clay adsorption of chloride-metal ion pairs in seawater. *Aquatic Geochemistry*, **11**, 115–137.

Cuadros, J. (1997) Interlayer cation effects on the hydration state of smectite. *American Journal of Science*, **297**, 829–841.

Di Leo, P. and Cuadros, J. (2003) Cd-113, H-1 MAS NMR and FTIR analysis of Cd^{2+} adsorption on dioctahedral and trioctahedral smectite. *Clays and Clay Minerals*, **51**, 403–414.

Di Leo, P. and O'Brien, P. (1999) Nuclear magnetic resonance (NMR) study of Cd^{2+} sorption on montmorillonite. *Clays and Clay Minerals*, **47**, 761–768.

Dickens, B. and Brown, W.E. (1972) The crystal structure of $CaKAsO_4.8H_2O$. *Acta Crystallographica*, **B28**, 3056–3065.

Drits, V.A. and Sakharov, B.A. (1976) *X-ray structure analysis of mixed-layer minerals*. *Doklady Akademii Nauk SSSR*, Moscow, 256 pp.

Drits, V.A. and Tchoubar, C. (1990) *X-ray diffraction by disordered lamellar structures: Theory and applications to microdivided silicates and carbons*. Springer-Verlag, Berlin, 371 pp.

Drits, V.A., Sakharov, B.A., Lindgreen, H. and Salyn, A. (1997a) Sequential structure transformation of illite-smectite-vermiculite during diagenesis of Upper Jurassic shales from the North Sea and Denmark. *Clay Minerals*, **32**, 351–371.

Drits, V.A., Środoń, J. and Eberl, D.D. (1997b) XRD measurement of mean crystallite thickness of illite and

illite/smectite: reappraisal of the Kübler index and the Scherrer equation. *Clays and Clay Minerals*, **45**, 461–475.

Elprince, A.M., Vanselow, A.P. and Sposito, G. (1980) Heterovalent, ternary cation exchange equilibria: NH^{4+}-Ba^{2+}-La^{3+} exchange on montmorillonite. *Soil Science Society of America Journal*, **44**, 964–969.

Ferrage, E., Lanson, B., Sakharov, B.A. and Drits, V.A. (2005a) Investigation of smectite hydration properties by modeling of X-ray diffraction profiles. Part 1. Montmorillonite hydration properties. *American Mineralogist*, in press.

Ferrage, E., Lanson, B., Malikova, N., Plançon, A., Sakharov, B.A. and Drits, V.A. (2005b) New insights on the distribution of interlayer water in bi-hydrated smectite from X-ray diffraction profile modeling of 00l reflections. *Chemistry of Materials*, **17**, 3499–3512.

Ferrage, E., Lanson, B., Sakharov, B.A., Geoffroy, N., Jacquot, E. and Drits, V.A. (2006) Investigation of smectite hydration properties by modeling of X-ray diffraction profiles. Part 2. Influence of layer charge and charge location. *American Mineralogist*, in prep.

Fletcher, P. and Sposito, G. (1989) The chemical modeling of clay/electrolyte interactions for montmorillonite. *Clay Minerals*, **24**, 375–391.

Guinier, A. (1964) *Théorie et technique de la radiocristallographie*. Dunod, Paris, 740 pp.

Hewish, N.A., Neilson, G.W. and Enderby, J. (1982) Environment of Ca^{2+} ions in aqueous solvent. *Nature*, **297**, 138–139.

Howard, S.A. and Preston, K.D. (1989) Profile fitting of powder diffraction patterns. Pp. 217–275 in: *Modern Powder Diffraction* (D.L. Bish and J.E. Post, editors). Reviews in Mineralogy **20**, Mineralogical Society of America, Washington, D.C.

Hyun, S.P., Cho, Y.H., Kim, S.J. and Hahn, P.S. (2000) Cu(II) sorption mechanism on montmorillonite: an electron paramagnetic resonance study. *Journal of Colloid and Interface Science*, **222**, 254–261.

Kittrick, J.A. (1969a) Interlayer forces in montmorillonite and vermiculite. *Soil Science Society of America Journal*, **33**, 217–222.

Kittrick, J.A. (1969b) Quantitative evaluation of the strong-force model for expansion and contraction of vermiculite. *Soil Science Society of America Journal*, **33**, 222–225.

Kodama, H., Gatineau, L. and Méring, J. (1971) An analysis of X-ray diffraction line profiles of microcrystalline muscovites. *Clays and Clay Minerals*, **19**, 405–413.

Laird, D.A. (1996) Model for crystalline swelling of 2:1 phyllosilicates. *Clays and Clay Minerals*, **44**, 553–559.

Laird, D.A. (1999) Layer charge influences on the hydratation of expandable 2:1 phyllosilicates. *Clays and Clay Minerals*, **47**, 630–636.

Madejová, J., Bujdak, J., Petit, S. and Komadel, P. (2000) Effects of chemical composition and temperature of heating on the infrared spectra of Li-saturated dioctahedral smectites. (II) Near-infrared region. *Clay Minerals*, **35**, 753–761.

Mazzarella, L., Kovacs, A.L., De Santis, P. and Liquori, A.M. (1967) Three-dimensional X-ray analysis of the complex $CaBr_2.10H_2O.2(CH_2)_6N_4$. *Acta Crystallographica*, **22**, 65–74.

Méring, J. (1949) L'interférence des rayons-X dans les systèmes à stratification désordonnée. *Acta Crystallographica*, **2**, 371–377.

Mermut, A.R. and Lagaly, G. (2001) Baseline studies of The Clay Minerals Society Source Clays: layer-charge determination and characteristics of those minerals containing 2:1 layers. *Clays and Clay Minerals*, **49**, 393–397.

Mooney, R.W., Keenan, A.G. and Wood, L.A. (1952) Adsorption of water vapor by montmorillonite. II. Effect of exchangeable ions and lattice swelling as measured by X-ray diffraction. *Journal of the American Chemical Society*, **74**, 1331–1374.

Moore, D.M. and Reynolds, R.C., Jr (1997) *X-ray Diffraction and the Identification and Analysis of Clay Minerals*. Oxford University Press, Oxford and New York, 322 pp.

Nagelschmidt, G. (1936) The structure of montmorillonite. *Zeitschrift für Kristallographie*, **93**, 481–487.

Norrish, K. (1954) The swelling of montmorillonite. *Discussions of the Faraday Society*, **18**, 120–134.

Plançon, A. (2002) New modeling of X-ray diffraction by disordered lamellar structures, such as phyllosilicates. *American Mineralogist*, **87**, 1672–1677.

Rhue, R.D. and Reve, W.H. (1990) Exchange capacity and adsorbed-cation charge as affected by chloride and perchlorate. *Soil Science Society of America Journal*, **54**, 705–708.

Sakharov, B.A., Lindgreen, H., Salyn, A. and Drits, V.A. (1999) Determination of illite-smectite structures using multispecimen X-ray diffraction profile fitting. *Clays and Clay Minerals*, **47**, 555–566.

Schlegel, M., Manceau, A., Charlet, L. and Hazemann, J.L. (2001) Adsorption mechanisms of Zn on hectorite as a function of time, pH, and ionic strength. *American Journal of Science*, **301**, 798–830.

Shainberg, I., Oster, J.D. and Wood, J.D. (1980) Sodium/calcium exchange in montmorillonite and illite suspension. *Soil Science Society of America Journal*, **44**, 960–964.

Spohr, E., Palinkas, G., Heinzinger, K., Bopp, P. and Probst, M.M. (1988) A molecular dynamics study of an aqueous $SrCl_2$ solution. *Journal of Physical Chemistry*, **92**, 6754.

Sposito, G. (1977) The Gapon and Vanselow selectivity coefficients. *Soil Science Society of America Journal*, **41**, 1205–1206.

Sposito, G. (1981) *The Thermodynamics of Soil Solution*. Oxford University Press, New York.

Sposito, G. (1984) *Surface Chemistry of Soils*. Oxford University Press, New York, 223 pp.

Sposito, G. (1991) Effect of chloride on sodium-calcium and sodium-magnesium exchange on montmorillonite. *Soil Science Society of America Journal*, **55**, 965–967.

Sposito, G., Holtzclaw, K.M., Johnston, C.T. and Le Vesque, C.S. (1981) Thermodynamics of sodium-copper exchange on Wyoming bentonite at 298 K. *Soil Science Society of America Journal*, **45**, 1079–1084.

Sposito, G., Holtzclaw, K.M., Charlet, L., Jouany, C. and Page, A.L. (1983a) Sodium-calcium and sodium-magnesium exchange on Wyoming bentonite in perchlorate and chloride background ionic media. *Soil Science Society of America Journal*, **47**, 51–56.

Sposito, G., Holtzclaw, K.M., Jouany, C. and Charlet, L. (1983b) Cation selectivity in sodium-calcium, sodium-magnesium, and calcium-magnesium exchange on Wyoming bentonite at 298 K. *Soil Science Society of America Journal*, **47**, 917–921.

Stucki, J.W., Golden, D.C. and Roth, C.B. (1984) Effects of reduction and reoxidation of structural iron on the surface charge dissolution of dioctahedral smectites. *Clays and Clay Minerals*, **32**, 350–356.

Suarez, D.L. and Zahow, M.F. (1989) Calcium-magnesium exchange selectivity of Wyoming montmorillonite in chloride, sulfate and perchlorate solutions. *Soil Science Society of America Journal*, **53**, 52–57.

Tournassat, C., Greneche, J.M., Tisserand, D. and Charlet, L. (2004a) The titration of clay minerals. Part I. Discontinuous backtitration technique combined to CEC measurements. *Journal of Colloid and Interface Science*, **273**, 224–233.

Tournassat, C., Ferrage, E., Poinsignon, C. and Charlet, L. (2004b) The titration of clay minerals. Part II. Structural-

based model and implications for clay reactivity. *Journal of Colloid and Interface Science*, **273**, 234–246.

Van Olphen, H. (1965) Thermodynamics of interlayer adsorption of water in clays. *Journal of Colloid Science*, **20**, 822–837.

Vanselow, A.P. (1932a) Equilibria of the base-exchange reaction of bentonites, permutites, soil colloids and zeolites. *Soil Science*, **33**, 95–113.

Vanselow, A.P. (1932b) The utilization of the base-exchange reaction for the determination of activity coefficients in mixed electrolytes. *Journal of the American Chemical Society*, **54**, 1307–1311.

Vantelon, D., Pelletier, M., Michot, L.J., Barres, O. and Thomas, F. (2001) Fe, Mg and Al distribution in the octahedral sheet of montmorillonites. An infrared study in the OH-bending region. *Clay Minerals*, **36**, 369–379.

Walker, G.F. (1956) The mechanism of dehydration of Mg-vermiculite. *Clays and Clay Minerals*, **4**, 101–115.

(*Received 10 May 2004; revised 21 February 2005; Ms. 912; A.E. David A. Laird*)